



HAL
open science

A stochastic approach for modelling airborne lidar waveforms

Clément Mallet, Florent Lafarge, Frédéric Bretar, Michel Roux, Uwe Soergel,
Christian Heipke

► **To cite this version:**

Clément Mallet, Florent Lafarge, Frédéric Bretar, Michel Roux, Uwe Soergel, et al.. A stochastic approach for modelling airborne lidar waveforms. *Laserscanning*, Sep 2009, Paris, France. hal-02384727

HAL Id: hal-02384727

<https://hal.science/hal-02384727v1>

Submitted on 28 Nov 2019

HAL is a multi-disciplinary open access archive for the deposit and dissemination of scientific research documents, whether they are published or not. The documents may come from teaching and research institutions in France or abroad, or from public or private research centers.

L'archive ouverte pluridisciplinaire **HAL**, est destinée au dépôt et à la diffusion de documents scientifiques de niveau recherche, publiés ou non, émanant des établissements d'enseignement et de recherche français ou étrangers, des laboratoires publics ou privés.

A STOCHASTIC APPROACH FOR MODELLING AIRBORNE LIDAR WAVEFORMS

Clément Mallet¹, Florent Lafarge², Frédéric Bretar¹, Michel Roux³, Uwe Soergel⁴, Christian Heipke⁴

¹ Laboratoire MATIS, Institut Géographique National, France – firstname.lastname@ign.fr

² IMAGINE, Université Paris Est, France – lafargef@imagine.enpc.fr

³ Département TSI, Telecom ParisTech, France – michel.roux@telecom.paristech.fr

⁴ Institut für Photogrammetrie und GeoInformation, Leibniz Universität Hannover, Germany – lastname@ipi.uni-hannover.de

Commission III - WG III/2

KEY WORDS: LIDAR, Full-Waveform, Modelling, MCMC, Urban

ABSTRACT:

In contrast to conventional airborne multi-echo laser scanner systems, full-waveform (FW) lidar systems are able to record the entire emitted and backscattered signals of each laser pulse. Instead of clouds of individual 3D points, FW devices provide 1D profiles of the 3D scene, which allows gaining additional and more detailed observations of the illuminated surfaces. Indeed, lidar waveforms are signals consisting of a train of echoes where each of them corresponds to a scattering target of the Earth surface or a group of close objects leading to superimposed signals. Modelling these echoes with the appropriate parametric function is necessary to retrieve physical information about these objects and characterize their properties. Henceforth, the extracted parameters can be useful for subsequent object segmentation and/or classification. This paper presents a stochastic based model to reconstruct lidar waveforms in terms of a set of parametric functions. The model takes into account both a data term which measures the coherence between the proposed configurations and the waveforms, and a regularizing term which introduces physical knowledge on the reconstructed signal. We search for the best configuration of functions by performing a Reversible Jump Markov Chain Monte Carlo sampler coupled with a stochastic relaxation. Finally, the algorithm is validated on waveforms from several airborne lidar sensors, showing the suitability of the approach even when the traditional assumption of Gaussian decomposition of waveforms is invalid.

1 INTRODUCTION

Airborne laser scanning is an active remote sensing technique providing range data as georeferenced 3D point clouds. It enables fast, reliable, accurate, but irregular mapping of both terrain and elevated features such as the tree canopy and the ground underneath. The new technology of full-waveform lidar systems permits to record the backscattered signal for each transmitted laser pulse. FW lidar data yield more than a basic geometric representation of the Earth topography. Instead of clouds of individual 3D points, lidar devices provide 1D profiles of the 3D scene, which allows gaining further physical observations of the illuminated surfaces by morphological analysis (Mallet and Bretar, 2009). Indeed, each signal consists of a series of temporal modes (called *echoes*), where each of them corresponds to the reflection from a unique object or a superposition of the signal of several elements (called *scatterers*).

Since small-footprint laser scanners with waveform digitizers are becoming increasingly available, many studies have already been carried out to perform advanced signal processing and analysis. The advantage of off-line waveform processing is twofold. By designing its own signal fitting algorithm, an end-user can:

(i) Maximize the detection rate of relevant peaks within the waveforms. Additional echoes can be extracted in a more reliable way. Therefore, range measurements are more accurately determined and close objects better discriminated (Jutzi and Stilla, 2006, Barber and Mills, 2007, Kirchhof et al., 2008).

(ii) Decompose the waveforms by modelling each echo with a suitable parametric function. It was found that in general small-footprint lidar waveforms can be well modelled with a sum of Gaussian pulses (Wagner et al., 2006). The Gaussian assumption is a suitable trade-off between simplicity and uniqueness solution. The echo shape (amplitude and width) can be retrieved, providing relevant features for tree segmentation (Reitberger et al., 2008), classification in urban areas (Mallet et al., 2008), or

ground discrimination, leading to more accurate Digital Terrain Models (Doneus et al., 2008).

Nevertheless, two main drawbacks can be noticed with a Gaussian assumption. Peaks may be asymmetric and therefore cannot be correctly adjusted. The attenuation of the laser beam within the tree canopy leads to an asymmetric backscattered pulse in case of large or medium-footprint lidar sensors. The geometry of solid targets (sloped building roof with micro-geometry) or two very close objects can have a similar effect when analyzing small-footprint lidar waveforms in urban areas. Moreover, the full-waveform Gaussian observables directly link to the backscatter target cross-section but may be inefficient or less discriminative for object segmentation compared with traditional spatial features. For segmenting surfaces (same coarse geometry but with distinct roughnesses), unusual modelling parametric functions are bound to provide discriminative features.

The aim of this study is to investigate further lidar waveform processing by taking these two issues into account.

Non-linear least-squares methods (Hofton et al., 2000) or maximum likelihood approach using the Expectation Maximization (EM) algorithm (Persson et al., 2005) are typically used to fit the signal to a mixture of Gaussian functions. However, the gradient computation required in such models limits both the introduction of physical knowledge on the waveforms and the type of the chosen function. Stochastic approaches are very promising for addressing the issue of reconstructing lidar waveforms. These models have shown good potentialities for many applications in remote sensing data analysis such as the extraction of road networks (Lacoste et al., 2005), facade reconstruction (Ripperda, 2008) or 3D building reconstruction (Lafarge et al., 2008). Our method hypothesizes mixtures of various parametric functions representing the reconstructed echos. An energy is associated to each configuration and the global minimum is then found using a Reversible Jump Markov Chain Monte Carlo (RJCMCMC) algorithm (Green, 1995). Our model presents several interesting char-

acteristics compared to conventional waveform modelling techniques mentioned above:

- *Multiple function types* - It allows to deal with various types of parametric functions. By using a library of shapes, more accurate estimates are performed compared to classical approaches (Salas-González et al., 2009).

- *Lidar physical knowledge integration* - Complex prior information on lidar waveform characteristics can be introduced in the energy without having problems of convexity or/and continuity restrictions in the formulation of these interactions.

- *Efficient exploration of configuration spaces* - A RJMCMC sampler with relevant proposition kernels allows to avoid exhaustive explorations of continuous configuration spaces, and is particularly efficient when the number of functions is unknown. Generally speaking, the MCMC samplers offer good potentialities in signal reconstruction (Punskaya et al., 2002), e.g., lidar waveform estimate, for counting and locating the reflected returns from surfaces (Hernández-Marín et al., 2007).

The proposed model is formulated in Section 2 as well as the optimization procedure. Section 3 presents and motivates the chosen library for fitting lidar echoes. The algorithm is then validated on waveforms from various airborne lidar sensors and results are shown in a urban area in Section 4. Finally, conclusions and perspectives are drawn.

2 THE PROPOSED MODEL

A stochastic framework is used to model lidar waveforms by predefined parametric functions. Each configuration x of parametric functions is measured by an energy $U(x)$. This energy computes the consistence between the configuration x and the observed lidar waveform, and takes into account complex interactions between the parametric functions x_i (called *objects*) of the configuration x . The energy minimization is complex in such a case since (i) we do not know the number of objects in the configuration, (ii) the objects are defined by a different number of parameters because there are various object types, and (iii) the energy is not convex. Most of conventional optimization algorithms cannot be performed in such conditions. A stochastic sampler detailed further is used to find the global minimum of U .

2.1 Energy formulation

The energy $U(x)$ measuring the quality of a configuration x is composed of both a data term $D(x)$ and a regularization one $R(x)$ such as:

$$U(x) = \beta D(x) + (1 - \beta) R(x) \quad (1)$$

where $\beta \in [0, 1]$ tunes the trade-off between the data and the prior terms.

2.1.1 Data energy D This term helps the model to best fit to the lidar waveforms. The likelihood can then be obtained by computing a distance between the given signal $\mathcal{S}_{\text{data}}$ and the estimated one \mathcal{S}_x , which depends on the current objects on the configuration x .

$$D(x) = \sqrt{\frac{1}{|K|} \int_K (\mathcal{S}_x - \mathcal{S}_{\text{data}})^2} \quad (2)$$

where K is the signal support. This term measures the quadratic error between both signals. It allows to be sensitive to high variations corresponding to local strong errors in signal estimates.

2.1.2 Prior $R(x)$ introduces interactions between objects of x , and favors or penalizes some configurations. For airborne lidar waveforms, the prior knowledge is set up by physical limitations

in the backscatter of lidar pulses. These limitations are modelled by three terms R_1 , R_2 , and R_3 .

$$R(x) = R_1(x) + R_2(x) + \sum_{x_i \sim x_j} R_3(x_i, x_j) \quad (3)$$

where $x_i \sim x_j$ constitutes the set of neighboring objects in the configuration x . This neighborhood relationship \sim is defined as follows:

$$x_i \sim x_j = \{(x_i, x_j) \in x \mid |\mu_{x_i} - \mu_{x_j}| \leq r\} \quad (4)$$

where μ_{x_i} (resp. μ_{x_j}) represents the mode (position of the maximum amplitude of the echo) of the associated function to object x_i (resp. x_j), and r is linked to the lidar sensor range resolution.

(i) Echo number limitation From our own observations, even for complex targets like forested areas, a waveform empirically reaches a maximum of seven echoes and it is rare to find more than four echoes. In urban areas, most of the targets are rigid, opaque structures like buildings and streets. Thus, more than two echoes are usually found in non dense trees. We then aim to favor configurations with a limited number of objects with an energy given by:

$$R_1(x) = -\log P_{\text{card}(x)} \quad \text{with} \quad \sum_{n=0}^{\infty} P_n = 1 \quad (5)$$

where P_n is the probability for the waveform to have n echoes. The probabilities are empirically set up by a coarse mode estimate on a urban test area (112M waveforms over 40 km²). Here, we have: $P_1 = 0.6$, $P_2 = 0.27$, $P_3 = 0.1$ and $P_{4 \leq n \leq 7} = 0.01$. For $n > 7$, $R_1(x) = +\infty$: it prevents the algorithm from choosing such configurations.

(ii) Backscattered energy limitation A laser scanning system receives a signal with a bounded energy. This upper bound depends on the emitted energy (which is commonly unknown), the target reflectance, and scattering properties. This reference power E_{ref} can be set empirically to $\sqrt{2\pi} A_{\text{max}} \sigma_{\text{max}}$. A_{max} and σ_{max} are upper bounds respectively for the amplitude and the width of echoes within the waveforms over the area of interest. Only waveforms with superior energy are as follows penalized.

$$R_2(x) = \omega_e \mathbb{1}_{\{E(x) > E_{\text{ref}}\}} (E(x) - E_{\text{ref}})^2 \quad (6)$$

where $\mathbb{1}_{\{\cdot\}}$ is the characteristic function, $E(x) = \int_K \mathcal{S}_x$ is the intensity of the configuration x , compared to the given reference power.

(iii) Sensor resolution limitation We aim to penalize objects closer than the sensor range resolution. Such energy is given by:

$$R_3(x_i, x_j) = \omega_m \exp\left(\frac{r^2 - |\mu_{x_i} - \mu_{x_j}|^2}{\sigma^2}\right) \quad (7)$$

It also favors configurations with a small number of objects. Indeed, a single pulse can be fitted by an important number of peaks that will not represent physical scatterers. Nevertheless, such configuration does not reflect the reality, and leads to results useless for target discrimination.

Physical and weight parameters can be distinguished in the energy. Physical parameters are r and σ . Small-footprint airborne topographic sensor specifications lead to $r = 5$ ns and we set σ to 0.01 ns. Thus, $R_3(x_i, x_j) \rightarrow +\infty$ when $\mu_{x_i} \rightarrow \mu_{x_j}$ Data and regularization terms are weighted one compared to the other, respectively with a factor β set to 0.5. The two prior weights ω_e and ω_m are tuned by “trial-and-error” tests.

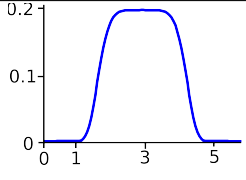
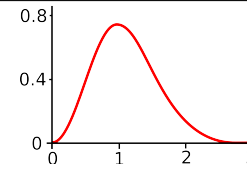
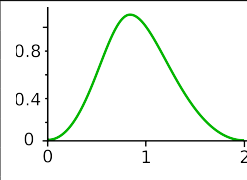
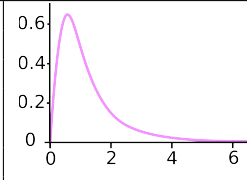
Model	Generalized Gaussian	Weibull	Nakagami	Burr
Parameters	I, s, σ, α	I, s, k, λ	I, s, μ, ω	I, s, a, b, c
Expression	$I \exp\left(-\frac{(x-s)\alpha^2}{2\sigma^2}\right)$	$I \frac{k}{\lambda} \left(\frac{x-s}{\lambda}\right)^{k-1} \times \exp\left(-\left(\frac{x-s}{\lambda}\right)^k\right)$	$I \frac{2\mu^\mu}{\omega\Gamma(\mu)} \left(\frac{x-s}{\omega}\right)^{2\mu-1} \times \exp\left(-\mu\left(\frac{x-s}{\omega}\right)^2\right)$	$I \frac{bc}{a} \left(\frac{x-s}{a}\right)^{-b-1} \times \left(1 + \left(\frac{x-s}{a}\right)^{-b}\right)^{-c-1}$
Shape	 $I=1, s=3, \sigma=2, \alpha=3$	 $I=1, s=0, k=2, \lambda=1$	 $I=1, s=0, \mu=2, \omega=1$	 $I=1, s=0, a=1, b=2, c=1$

Table 1: Library of models. I and s are common parameters to all functions, respectively for amplitude and shift or location.

2.2 Optimization by Monte Carlo sampling

We aim to find the configuration of objects which minimizes the non convex energy U in a variable dimension space. Indeed, the number of objects is unknown and function types are defined by different number of parameters (see Table 1). Such a space can be efficiently explored using a Reversible Jump Markov Chain Monte Carlo (RJMCMC) sampler (Green, 1995) coupled with a stochastic relaxation. One of the advantage of this iterative algorithm is that it does not depend on the initial state. Object configurations are sampled according to families of moves called proposition kernels and denoted by Q_m where m represents the family of moves. The sampler performs a move from an object configuration x to y according to a probability $Q_m(x \rightarrow y)$. Then, the move is accepted with the following probability:

$$\min \left(1, \frac{Q_m(y \rightarrow x)}{Q_m(x \rightarrow y)} \exp - \frac{(U(y) - U(x))}{T} \right) \quad (8)$$

where T is the relaxation parameter. We use three different families of moves ($m = \{1, 2, 3\}$):

- **Perturbation kernel** Q_1 : a parameter of an object belonging to the current configuration x is modified;
- **Birth-and-death kernel** Q_2 : an object is added or removed from the current configuration x and
- **Switching kernel** Q_3 : the type of an object belonging to x is switched with another type of the library.

The probabilities of choosing each move are equal since no assumption can be made on which move is more relevant at the current state. More details concerning this optimization technique are given in (Green, 1995).

3 SET OF MODELLING FUNCTIONS

The contents of the library is a key point since the function parameters will be used afterwards for classifying 3D point clouds. The Gaussian and Generalized Gaussian (GG) models have been shown to fit most of the echoes of small-footprint lidar waveforms in urban areas (Wagner et al., 2006, Chauve et al., 2007). Nevertheless, this assumption is not always sufficient. Non unique asymmetric echoes are observed within waveforms corresponding to echoes slightly skewed by roof materials, ground surface or tree canopy. The GG model gives the amplitude, width, and shape for symmetric echoes. Amplitude and width are useful for discriminating ground, vegetation and buildings (Gross et al., 2007, Wagner et al., 2008) but fail segmenting different kinds of surfaces such as grass, gravel and asphalt (Mücke, 2008), even when the pulse shape is available (Mallet et al., 2008). The backscattered cross-section gives slightly better discrimination (Mücke, 2008).

Two kinds of functions must therefore be included: functions

able to fit asymmetric peaks and those which can simulate both skewed and non-skewed echoes with other parameters than provided by the Gaussian/GG models.

Thus, three new functions are introduced. The **Weibull** distribution provides a scale and a shape parameter offering the possibility to simulate symmetric or asymmetric peaks with two new parameters. The **Nakagami** distribution is a generalization of the Chi distribution and can simulate right-skewed distributions with a skewness parameter. Finally, the **Burr** function simulates specifically asymmetric modes with two shape parameters. Table 1 summarizes the analytical expressions as well as the parameters of each distribution of the library. Weibull and Nakagami functions are traditionally used to model Synthetic Aperture Radar (SAR) images to estimate their amplitude probability density functions as well as for subsequent classification (Tison et al., 2004). For airborne lidar waveforms, there is no physical background justifying their use. Despite this fact, these models may outperform the Gaussian assumption in many cases and enhance lidar waveform analysis and classification.

This library is not exhaustive. The final choice of modelling functions will depend on the relevance of their parameters for the selected classes. A parameter is relevant whether it improves classification results. This choice is totally independent of the stochastic approach presented here (feature selection step).

4 RESULTS

The algorithm has been carried out on different kinds of airborne lidar signals. A waveform-by-waveform evaluation to both estimate its quality and the correctness of the echo detection would be highly time-consuming. Thus, it has been rather evaluated by computing the correlation coefficient ρ and the relative Kolmogorov-Smirnov distance KS between the raw and the estimated signals. KS is a L_∞ norm based indicator, used to detect missing echoes and defined as follows:

$$KS(\mathcal{S}_{\text{data}}, \mathcal{S}_{\text{final}}) = \frac{\sup_K |\mathcal{S}_{\text{data}} - \mathcal{S}_{\text{final}}|}{\max_K \mathcal{S}_{\text{data}}} \quad (9)$$

where $\mathcal{S}_{\text{final}}$ is the final estimated signal.

4.1 Experiments on simulated signals

The algorithm has been first applied on signals with a higher complexity than real lidar waveforms to assess its effectiveness. Longer signals with more echoes than physically expected, with distorted and overlapping modes as well as corrupted with noise have been fitted with our method. The prior physical parameters have just to be tuned to extend the energetical formulation to other kinds of signals. To deal respectively with very close echoes and with large overlapping ones, the interaction between objects can

be changed by decreasing and increasing r and σ . To reconstruct signals with higher energy, E_{ref} can be tuned. To fit signals with more modes, the echo number limitation can be modified by accepting more echoes within the signal and, for instance, with the same probability.

Figure 1 shows that good fitting results can be achieved on simulated waveforms, even corrupted with Gaussian noise. The waveform is composed of nine peaks: three single echoes and three pairs of overlapping echoes. The nine echoes are retrieved and their locations accurately found. However, small differences between the reference and the estimated signals can be locally noticed, especially with noisy signals. The algorithm has more difficulties to find the exact maxima and fit the upper parts of the modes (e.g., 2nd and 4th echoes in Figure 1).

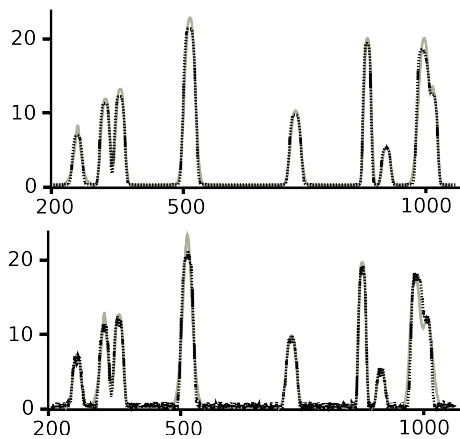


Figure 1: Results of complex waveform fitting on a simulated signal with nine echoes (**above**) and on the same signal with Gaussian noise (**below**). The dotted black line and the continuous grey one are respectively the raw and the reconstructed signals.

4.2 Experiments on waveforms from different lidar sensors

Several lidar sensors provide signals of backscattered laser pulses. Their specifications can be found in (Mallet and Bretar, 2009). Such waveforms can be reconstructed and their echoes modelled with our approach showing its flexibility. One just has to tune the prior parameters. Depending on the surveyed area, the echo number limitation term of the energy can be discarded or become more restrictive. Moreover, the range resolution parameters (r and σ) can be changed according to the sensor specifications and the adopted classification strategy. For instance, with medium or large-footprint waveforms, it should be sufficient to fit overlapping echoes with a single function to retrieve a “global” return of the tree canopy or the ground.

4.2.1 Bathymetric waveforms Green lidar waveforms are used in bathymetry for accurate sea/river-depth estimates. They are ideally composed of two echoes corresponding respectively for the first and second echoes to the air-water boundary and the seafloor. First echoes are skewed due to the scattering and spreading of pulse at the sea surface. For second echoes, the received power from the bottom decreases exponentially with the water depth and the attenuation coefficient, and thus cannot be fitted with a Gaussian model. They can be represented by an exponential decaying function that should be introduced in future works. Our algorithm has been tested on waveforms acquired in June 2005 on a near-shore area of 300 km² of the Morbihan Gulf (France), using a SHOALS 1000T device. The waters are particularly shallow. Thus, the provided signals consist of one or two overlapping peaks. Table 2 summarizes the modelling statistics

¹Data set available at <https://lvis.gsfc.nasa.gov/index.php>

on 190 waveforms. The quality measures ρ and KS show that the signals are correctly reconstructed and only few peaks are missed. They correspond to superimposed peaks. First echoes of two-mode waveforms are modelled both by the GG and Nakagami functions. However, first and second peaks are too close located to deduce that they correspond to symmetric echoes. Moreover, the second peaks are mainly adjusted by asymmetric models. The Weibull function has been barely selected by the algorithm. No conclusions can be drawn on the fitted waveforms since such model has a similar behaviour to the Nakagami one.

Echo	ρ	KS	GG	Weibull	Naka.	Burr
First	0.97	0.1	55.5	0.5	39.2	4.8
Second			3.8	0.1	54.4	41.7

Table 2: Fitting quality measures and statistics on echo modelling for 190 bathymetric waveforms (SHOALS 1000T).

4.2.2 Airborne medium and large-footprint topographic waveforms

The return waveforms of large-sized footprint lidar sensors give the record of the vertical distribution of intercepted elements in a large conical region of the 3D space. This leads to non Gaussian statistics of object elevations within the diffraction cone. Such right-skewed waveforms can also be noticed with medium-footprint waveforms, especially in vegetated areas. This is due to the attenuation of the laser beam within the tree canopy. The Beer-Lambert law states the energy exponentially decreases while increasing the target range and the absorption coefficients.

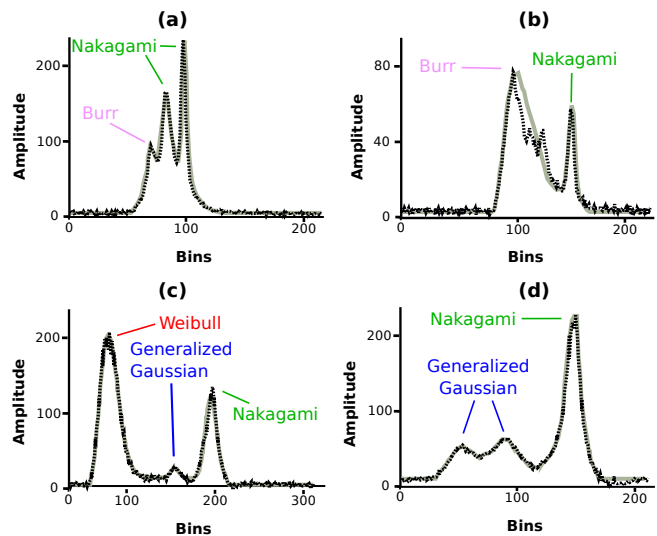


Figure 2: Examples of adjusted (a-b) LVIS and (c-d) SLICER waveforms.

Waveforms from SLICER and LVIS lidar sensors have been decomposed and modelled with our approach (Figure 2). LVIS waveforms have been acquired in March 1998 over a 800 km² area of Costa Rica using 25 m-diameter footprints as part of the pre-launch activities of the Vegetation Canopy Lidar (VCL) Mission¹ (Hofton et al., 2002). Both fine and coarse fitting strategies have been tested. The fine strategy consists in selecting r according to the sensor resolution $r = 20$ ns (10 bins). It leads to almost perfect signal fitting but conclusions are difficult to draw since the function selected for a given peak depends on the functions of the neighboring echoes (Figure 2a). With the coarse solution, r is set to 60 ns (30 bins) and σ to 0.001 ns. It prevents overlapping or close echoes from being individually fitted. A unique global peak is selected instead (Figure 2b), providing a general trend for the first part of the signal. SLICER elevation profiles come from

in the BOREAS Northern Study Area in Canada², and have been acquired in July 1996 (Harding, 2000). Table 3 shows that signals from both sensors are correctly decomposed but with less accuracy than bathymetric and small-footprint waveforms. Compared to the latter ones, SLICER and LVIS elevation profiles are much more complex since the sensor laser beam integrates a significant number of distinct objects (see Figure 2b). With medium and large-footprint waveforms, the Generalized Gaussian model is no longer selected by the algorithm. The three functions enabling to simulate asymmetric peaks are equally preferred. The main noticeable results are that the GG function is chosen for peaks with a small amplitude and that the Nakagami one is mainly selected for the last echo, which correspond to the ground and low above-ground objects.

Sensor (# WFs)	ρ	KS	GG	Weibull	Naka.	Burr
SLICER (340)	0.956	0.22	1.5	26.5	31.4	40.6
LVIS (333)	0.971	0.2	2.7	37.8	23.4	36.1

Table 3: Medium and large-footprint waveform fitting and modelling statistics. The fine solution has been adopted for the signal decomposition.

4.3 Airborne topographic small-footprint lidar waveforms in urban areas

Waveforms acquired from small-footprint airborne lidar systems (Riegl LMS-Q560 and Optech 3100EA) over various kinds of landscapes have been fitted using the stochastic approach. Figure 3 shows results both on urban and natural items. The right number of echoes is found as well as the correct shape of the waveform: single and multiple overlapping echoes are retrieved, even in vegetated areas where the noise level is significant w.r.t. the echo amplitudes (Figures 3a and b).

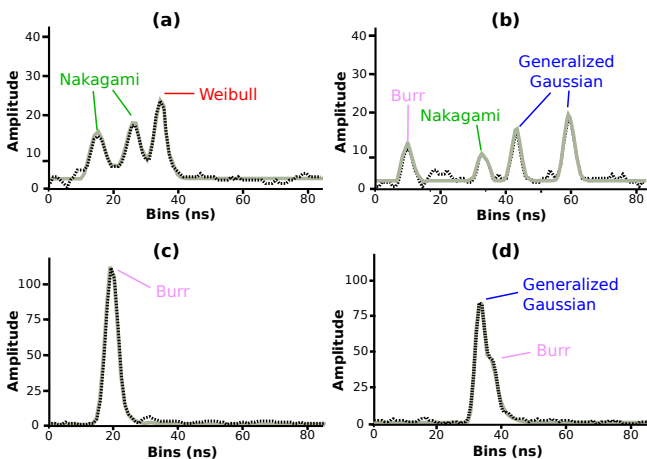


Figure 3: Decomposed and modelled waveforms on (a-b) trees, (c) a building roof, and (d) a hedge (Riegl LMS-Q560 sensor).

The Generalized Gaussian, Weibull and Nakagami functions have been introduced to model the same kind of echoes. Thus, there is no concluding whether the minimal configurations obtained are composed of the right modelling functions. As expected, the Burr model allows to fit slightly asymmetric echoes, especially the second echo of two overlapping ones (Figures 3c and d). Approximately 3000 waveforms acquired with the Optech 3100EA sensor over a urban area have been analysed. The aim

is to assess the reliability of the method in heterogeneous landscapes and to show its local stability in homogeneous areas. Three regions of interest have been selected: a flat harvested field (*Field*), a flat mixed asphalt/grass surface with a single tree (*Ground*), and a building with grass and pavements (*Building*). All the waveforms have been acquired in the nadir view or with a small angle of incidence. Table 4 shows that with small-footprint waveforms (*i.e.*, with signals composed of distinct echoes with non complex shapes) the fitting accuracy is high ($\rho > 0.99$ and $KS < 0.06$). For flat areas, in the nadir view, the echoes are symmetric. Thus, as expected, the Generalized Gaussian function is selected for most of the waveforms, except for some echoes within the tree canopy for the *Ground* region. Nevertheless, since for this area, the Burr function is almost never chosen (one waveform among 1535). It can be concluded that, in reality, all the waveform have symmetric echoes. Asymmetric modelling functions are therefore irrelevant for fitting echoes of small-footprint waveforms in vegetated areas. The Gaussian function is therefore sufficient and its parameters more convenient for modelling and estimating the influence of hit targets on the i^{th} echo of a waveform (Wagner et al., 2008). Finally, for the building region, both symmetric and skewed peaks are retrieved. Asymmetric echoes can be found on the building roof as well as on its edge, and where small surface discontinuities exist (see Figure 4).

Area (# WFs)	ρ	KS	GG	Weibull	Naka.	Burr
Field (936)	0.996	0.032	99.7	0	0.2	0.1
Ground (1535)	0.991	0.059	95.9	2.91	1.13	0.07
Building (544)	0.995	0.039	54.3	0.9	30.1	14.7

Table 4: Fitting results on three urban regions of interest (Optech 3100EA sensor).

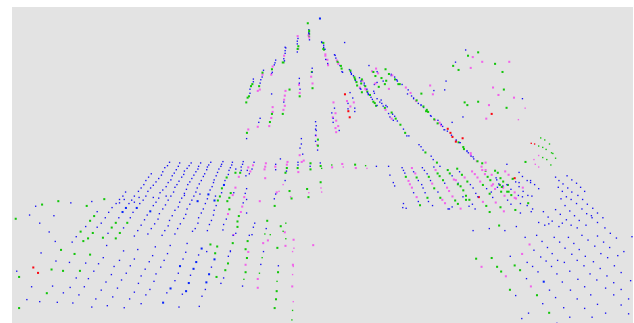


Figure 4: 3D point cloud labelled with the model selected by the stochastic approach (*Building* area). The colors are those of Table 1.

5 CONCLUSIONS AND FUTURE WORK

We have proposed an original method for modelling lidar waveforms by complex parametric functions. The obtained results are satisfactory and no lost of fitting accuracy is noticed compared to a classical Gaussian waveform fitting scheme. The stochastic approach is well adapted both to locate echoes in signals and accurately describe them with parametric functions taken from the extensible and tunable model library. The algorithm has been successfully applied to waveforms from different lidar sensors, showing its effectiveness and flexibility from various landscapes and footprints. For medium and large-sized footprints, the chosen

²Data set available at <http://core2.gsfc.nasa.gov/research/laser/slicer/browser.html>

functions allow to adjust asymmetric peaks when necessary. Furthermore, the low rate of Gaussians can be noticed and justifies the interest of the approach. For small-footprints, the skewness of the echoes is less significant. All of the models, except the Burr one are suitable. The potential advantages of this approach are therefore twofold. 3D points can be generated over large areas, on one hand, with shape descriptors that are the parameters of the modelling functions. This is almost relevant for non overlapping echoes which do not interact with each other in the energy minimization process. On the other hand, the 3D points can be labelled with their modelling function. By providing new features, our approach offers the possibility to improve classical lidar point cloud classification algorithm. Depending on the latter one, a feature selection step may be carried out to assess whether the extracted attributes will be discriminative.

Finally, in future works, it would be interesting to estimate automatically the weighting parameters using for instance the EM algorithm. Moreover, we should introduce in the energy formulation firstly specific interactions between parametric functions of different types in order to improve local signal adjustments. Eventually, since consecutive small-footprint waveforms along a scan line and in the orthogonal directions are likely to have similar shapes, spatial interactions should also be included in the regularization term of the proposed model.

ACKNOWLEDGEMENTS

LVIS data set was provided by the Laser Vegetation Imaging Sensor team in the Laser Remote Sensing Branch at NASA Goddard Space Flight Center with support from the University of Maryland, College Park. The authors would like to thank the SHOM for providing the bathymetric waveforms.

REFERENCES

- Barber, D. and Mills, J., 2007. Vehicule based waveform laser scanning in a coastal environment. *International Archives of Photogrammetry, Remote Sensing and Spatial Information Sciences* vol. 36, part 5/C55, pp. 35–40. Padua, Italy.
- Chauve, A., Mallet, C., Bretar, F., Durrieu, S., Pierrot-Deseilligny, M. and Puech, W., 2007. Processing full-waveform lidar data: modelling raw signals. *International Archives of Photogrammetry, Remote Sensing and Spatial Information Sciences* vol. 36, part 3/W52, pp. 102–107. Espoo, Finland.
- Doneus, M., Briese, C., Fera, M. and Janner, M., 2008. Archaeological prospection of forested areas using full-waveform airborne laser scanning. *Journal of Archaeological Science* 35(4), pp. 882–893.
- Green, P., 1995. Reversible Jump Markov Chain Monte-Carlo computation and Bayesian model determination. *Biometrika* 82(4), pp. 97–109.
- Gross, H., Jutzi, B. and Thoenessen, U., 2007. Segmentation of Tree Regions using Data of a Full-Waveform Laser. *International Archives of Photogrammetry, Remote Sensing and Spatial Information Sciences* vol. 36, part 3/W49A, pp. 57–62. Munich, Germany.
- Harding, D., 2000. BOREAS Scanning Lidar Imager of Canopies by Echo Recovery (SLICER): Level-3 Data. Available by special arrangement with Oak Ridge National Laboratory Distributed Active Archive Center, Oak Ridge, Tennessee, U.S.A. [<http://www.daac.ornl.gov>]. (on CD-ROM).
- Hernández-Marín, S., Wallace, A. and Gibson, G., 2007. Bayesian Analysis of Lidar Signals with Multiple Returns. *IEEE Transactions on Pattern Analysis and Machine Intelligence* 29(12), pp. 2170–2180.
- Hofton, M., Minster, J. and Blair, J., 2000. Decomposition of Laser Altimeter Waveforms. *IEEE Transactions on Geoscience and Remote Sensing* 38(4), pp. 1989–1996.

- Hofton, M., Rocchio, L., Blair, J. and Dubayah, R., 2002. Validation of Vegetation Canopy Lidar sub-canopy topography measurements for a dense tropical forest. *Journal of Geodynamics* 34(3-4), pp. 491–502.
- Jutzi, B. and Stilla, U., 2006. Range determination with waveform recording laser systems using a Wiener Filter. *ISPRS Journal of Photogrammetry & Remote Sensing* 61(2), pp. 95–107.
- Kirchhof, M., Jutzi, B. and Stilla, U., 2008. Iterative processing of laser scanning data by full waveform analysis. *ISPRS Journal of Photogrammetry & Remote Sensing* 63(1), pp. 99–114.
- Lacoste, C., Descombes, X. and Zerubia, J., 2005. Point processes for unsupervised line network extraction in remote sensing. *IEEE Transactions on Pattern Analysis and Machine Intelligence* 27(2), pp. 1568–1579.
- Lafarge, F., Descombes, X., Zerubia, J. and Pierrot-Deseilligny, M., 2008. Building reconstruction from a single DEM. In: *IEEE Conference on Computer Vision and Pattern Recognition*, Anchorage, USA.
- Mallet, C. and Bretar, F., 2009. Full-waveform topographic lidar: State-of-the-art. *ISPRS Journal of Photogrammetry & Remote Sensing* 64(1), pp. 1–16.
- Mallet, C., Bretar, F. and Soergel, U., 2008. Analysis of Full-Waveform Lidar Data for Classification of Urban Areas. *Photogrammetrie Fernerkundung Geoinformation* 5, pp. 337–349.
- Mücke, W., 2008. Analysis of full-waveform airborne laser scanning data for the improvement of DTM generation. Master's thesis, Institut für Photogrammetrie und Fernerkundung, Technische Universität Wien, Austria. http://publik.tuwien.ac.at/files/PubDat_170289.pdf (accessed April 9, 2009).
- Persson, A., Söderman, U., Töpel, J. and Alhberg, S., 2005. Visualization and Analysis of Full-Waveform Airborne Laser Scanner Data. *International Archives of Photogrammetry, Remote Sensing and Spatial Information Sciences* vol. 36, part 3/W19, pp. 103–108. Enschede, the Netherlands.
- Punskaya, E., Andrieu, C., Doucet, A. and Fitzgerald, W., 2002. Bayesian curve fitting using MCMC with applications to signal segmentation. *IEEE Transactions on Signal Processing* 50(3), pp. 747–758.
- Reitberger, J., Schnörr, C., Krzystek, P. and Stilla, U., 2008. 3D segmentation of full-waveform lidar data for single tree detection using normalized cuts. *International Archives of Photogrammetry, Remote Sensing and Spatial Information Sciences* vol. 37, part 3A, pp. 77–83. Beijing, China.
- Ripperda, N., 2008. Grammar based facades reconstruction using rjMCMC. *Photogrammetrie Fernerkundung Geoinformation* 2, pp. 83–92.
- Salas-González, D., Kuruoglu, E. and Ruiz, D., 2009. Finite mixture of α -stable distributions. *Digital Signal Processing* 19(2), pp. 360–369.
- Tison, C., Nicolas, J.-M., Tupin, F. and Maitre, H., 2004. A New Statistical Model for Markovian Classification of Urban Areas in High-Resolution SAR Images. *IEEE Transactions on Geoscience and Remote Sensing* 42(10), pp. 2046–2057.
- Wagner, W., Hollaus, M., Briese, C. and Ducic, V., 2008. 3D vegetation mapping using small-footprint full-waveform airborne laser scanners. *International Journal of Remote Sensing* 29(5), pp. 1433–1452.
- Wagner, W., Ullrich, A., Ducic, V., Melzer, T. and Studnicka, N., 2006. Gaussian decomposition and calibration of a novel small-footprint full-waveform digitising airborne laser scanner. *ISPRS Journal of Photogrammetry & Remote Sensing* 60(2), pp. 100–112.